Kinetic energy density of nearly free electrons. II. Response functionals of the electron density

William C. Witt[1] and Emily A. Carter[2,*]

[1]*Department of Mechanical and Aerospace Engineering,Princeton University, Princeton, New Jersey 08544-5263, USA*

[2]*School of Engineering and Applied Science, Princeton University, Princeton, New Jersey 08544-5263, USA*

(Received 5 March 2019; published 3 September 2019)

We present electron-density-based response functionals yielding the non-negative kinetic energy density (KED) of nearly free electron systems. In a previous paper, for a canonical free-electron system perturbed by an external potential, we derived the first- and second-order corrections to the KED as functionals of the potential, providing the response functions in reciprocal space. Here, we formulate the KED response in terms of the electron density by converting the potential-based functionals into density functionals. We also determine the related response of the Pauli KED, which is the KED in excess of the von Weizsäcker KED. We anticipate that the structure of these density functionals will help guide the design of the more sophisticated kinetic energy functionals required for orbital-free density functional theory simulations. We conclude by examining the performance of the first- and second-order density functionals for the KED when applied to electron densities generated from local pseudopotential calculations for Li, Al, and Si crystals.

DOI: 10.1103/PhysRevB.100.125107

I. INTRODUCTION

In this paper, the second in a two-part series, we examine electron-density-based response functionals for the kinetic energy density (KED) of nearly free electron systems. Specifically, we consider the non-negative KED defined as

$$t(\mathbf{r}) = \tfrac{1}{2}[\nabla_{\mathbf{r}} \cdot \nabla_{\mathbf{r}_0} \gamma(\mathbf{r}, \mathbf{r}_0)]_{\mathbf{r}_0 \to \mathbf{r}}, \tag{1}$$

with $\gamma(\mathbf{r}, \mathbf{r}_0)$ representing the reduced density matrix for noninteracting electrons with Hamiltonian $\hat{H} = -\frac{1}{2}\nabla^2 + \hat{v}$, where $v(\mathbf{r})$ is a static external potential. [An alternate KED, $t_L(\mathbf{r}) = t(\mathbf{r}) - \frac{1}{4}\nabla^2 n(\mathbf{r})$, where $n(\mathbf{r})$ is the electron density, arises from another natural definition for the KED, but this quantity may become negative.] The response functionals we derive yield the KED that emerges after initially free electrons—having a uniform KED t_0—are subjected to a static perturbing potential. In the first paper (Part I) [1], we formulated the KED response using a standard potential functional approach.

Here, we convert those potential functionals into alternate density functionals, which depend exclusively on (1) the free-electron density of the unperturbed system and (2) the change in the electron density induced by the perturbation. We also obtain density functionals for the first- and second-order response of the Pauli KED [2,3], which is the quantity $t_P(\mathbf{r}) = t(\mathbf{r}) - t_{vW}[n](\mathbf{r})$, where

$$t_{vW}[n](\mathbf{r}) = \tfrac{1}{2}|\nabla\sqrt{n(\mathbf{r})}|^2 \tag{2}$$

is the non-negative von Weizsäcker KED [4]. The von Weizsäcker KED equals the exact KED for any single-orbital system and, defined in this manner, provides a local lower bound [3,5] to the exact KED for all systems; the Pauli KED is the non-negative excess amount attributable to the fermionic character of the electrons.

Before proceeding, we remark on one particular motivation for this work, which relates to the study of materials with density functional theory (DFT) calculations [6,7]. Orbital-free (OF) DFT [8–11] is an alternative to the conventional approach to Kohn-Sham (KS) DFT [7] in which the noninteracting kinetic energy of the electrons—that is, the integrated quantity, T_s, where $T_s = \int d\mathbf{r} t(\mathbf{r})$—is approximated directly with an explicit density functional rather than determined indirectly (but exactly) following the introduction of auxiliary single-particle wave functions. The OF approach offers a significant reduction in computational requirements—largely because it eliminates the need for wave functions altogether and naturally attains linear or quasilinear complexity scaling with increasing system size—enabling study of many thousands of atoms (or more), as well as efficient molecular dynamics simulations that remain grounded in the underlying laws of quantum mechanics.

The search for universally applicable density functional approximations for T_s that are both accurate and suitable for rapid computation has a long history [6,8–17]. A number of the most successful approximations leverage a known relationship between a second functional derivative of T_s and the Lindhard [18] function $\tilde{J}_1(\mathbf{k}_1, k_\mu)$, where the latter also appears in the potential functional for the first-order electron density [see Eqs. (79) and (80) in Part I]. The relationship is

$$\mathcal{F}\left[\left.\frac{\delta^2 T_s}{\delta n(\mathbf{r})\delta n(\mathbf{r}')}\right|_{n_0}\right] = -\frac{1}{\tilde{J}_1(\mathbf{k}_1, k_\mu[n_0])}, \tag{3}$$

where $\mathcal{F}[\bullet]$ denotes a Fourier transform, n_0 is the uniform electron density of a free-electron reference system, and $k_\mu[n_0] = (3\pi^2 n_0)^{1/3}$ is the Fermi wave vector for that system. Even from the earliest work on DFT [6,7], it was apparent that the Lindhard function can be a useful ingredient in

*eac@princeton.edu

approximate density functionals for DFT calculations. Pioneering embodiments of this philosophy [19–22], targeting T_s specifically, inspired a still-growing body of research that encompasses the incorporation of, to give a few examples, the generalization of Eq. (3) for the third functional derivative of T_s [20,23], the version of Eq. (3) that applies to the kinetic potential [24,25], and variations on Eq. (3) that are more appropriate for semiconducting systems [26,27].

However, functionals that approximate the integrated T_s using this strategy are not always able to respect known constraints on the local KED (or kinetic potential), such as the local lower bound provided by the von Weizsäcker KED that we highlighted above. Furthermore, a resurgence within a different category of functional approximations—see work by Constantin *et al.* [28] and Luo *et al.* [29] for two recent examples, and references therein—is partly attributable to rigorous satisfaction of local constraints, underscoring the utility of targeting the local $t(\mathbf{r})$.

One of the chief results given below—expressed in Eqs. (17)–(19)—may be understood as an analog of Eq. (3) for the local KED, providing the corresponding second functional derivative of $t(\mathbf{r})$ in an analytical form. Any approximation for $t(\mathbf{r})$ that is constructed to fulfill the requirement implied by Eqs. (17)–(19) will automatically respect the global constraint implied by Eq. (3)—and, in addition, could conceivably take full advantage of the accumulated wisdom relating to other local constraints. The best avenue for accomplishing this task, while preserving computational efficiency, is not immediately obvious; investigations of this sort are ongoing.

Finally, we note two additional reasons to consider response functionals for the local KED. First, explicit density functionals for the KED can be useful for implementing some exchange-correlation (XC) functionals requiring the KED as an ingredient [30–32]. Second, we expect response functionals for the KED to be useful for hybrid DFT approaches that use different approximation strategies in different regions of space [33,34].

In Sec. II, we summarize briefly the requisite aspects of Part I. In Sec. III, we describe the procedure for converting potential functionals into density functionals, and then give the first- and second-order density functionals for the KED response. These expressions are one contribution of this paper, as are the analogous expressions for the Pauli KED given in the same section. Next, in Sec. IV, we inspect effective external pseudopotentials along with the corresponding electron densities and KEDs for a few Li, Al, and Si crystals—and then assess the approximate KEDs predicted by the density functionals from Sec. III. Concluding remarks are in Sec. V. An appendix demonstrates that the response functional formalism can be used to recover the conventional gradient expansion for slowly varying densities (see Ref. [13] for an overview of the latter, and references therein).

II. BACKGROUND

We consider spin-unpolarized, noninteracting electrons, specifying that eigenstates of the Hamiltonian $\hat{H} = -\frac{1}{2}\nabla^2 + \hat{v}$ with energies below a chemical potential μ are each populated with two electrons. Below, in a subsequent section, we will consider KS electrons, obtained by treating the KS effective potential as a fixed external potential.

A. Free-electron systems and the Thomas-Fermi approximation

Free electrons are subject to the simpler Hamiltonian $\hat{H}_0 = -\frac{1}{2}\nabla^2 + v_0$, where v_0 is a constant. The electron density and KED of free-electron systems are nonzero only for $\mu > v_0$, in which case they are

$$\begin{Bmatrix} n_0 \\ t_0 \end{Bmatrix} = \begin{Bmatrix} k_\mu^3/(3\pi^2) \\ k_\mu^5/(10\pi^2) \end{Bmatrix}, \tag{4}$$

where $k_\mu = [2(\mu - v_0)]^{1/2}$ is the Fermi wave vector (in terms of the potential). One may use Eq. (4) to re-express t_0 as a function(al) of n_0 [see also the definition of $k_\mu[n_0]$ given after Eq. (3)], yielding $t_0[n_0] = c_0 n_0^{5/3}$ with $c_0 = (3/10)(3\pi^2)^{2/3}$. When, as an approximation, this result is applied locally to a nonuniform electron density,

$$t_{TF}[n](\mathbf{r}) = c_0 n^{5/3}(\mathbf{r}), \tag{5}$$

it is known as the Thomas-Fermi density functional for the KED [35,36], which becomes asymptotically exact in the limit of a slowly varying density. (In writing $t_0[n_0]$ and $t_{TF}[n](\mathbf{r})$, we use a bracket notation to distinguish these terms as density functionals rather than potential functionals.) The Thomas-Fermi potential functionals obtained by substituting $v_0 \to v(\mathbf{r})$ in Eq. (4) are traditionally understood to yield zero (by definition) in classically forbidden regions where $v(\mathbf{r}) > \mu$; if not, they would yield imaginary values. In contrast, the KED in Eq. (5) can be extended naturally into classically forbidden regions. Finally, after partitioning the electron density into a free part and a perturbation, $n(\mathbf{r}) = n_0 + n_\Delta(\mathbf{r})$, we record the Taylor series expansion of Eq. (5) about $n_\Delta(\mathbf{r}) = 0$ through second order:

$$t_{TF}[n](\mathbf{r}) \approx t_0[n_0] + \frac{k_\mu^2}{2} n_\Delta(\mathbf{r}) + \frac{\pi^2}{2k_\mu} n_\Delta(\mathbf{r})^2, \tag{6}$$

The first- and second-order coefficients in Eq. (6) reappear below, matching the full response functions for the limiting case of a slowly varying perturbation in the density.

B. Response functionals of the perturbing potential

Nearly free electrons are characterized by the Hamiltonian $\hat{H} = -\frac{1}{2}\nabla^2 + v_0 + v_\Delta(\mathbf{r})$, with $v_\Delta(\mathbf{r})$ treated as a perturbation. In Part I, we described the usual potential-functional approach for determining the response of free electrons to a static perturbing potential. Recalling the definition of $n_\Delta(\mathbf{r})$ given above, and introducing $t_\Delta(\mathbf{r}) = t(\mathbf{r}) - t_0$, the analogous deviation from the free-electron KED, this approach leads to the potential-functional series:

$$\begin{aligned} \begin{Bmatrix} n_\Delta(\mathbf{r}) \\ t_\Delta(\mathbf{r}) \end{Bmatrix} = & \int \frac{d\mathbf{k}_1}{(2\pi)^3} e^{i\mathbf{k}_1\cdot\mathbf{r}} \begin{Bmatrix} \tilde{J}_1(\mathbf{k}_1, k_\mu) \\ \tilde{K}_1(\mathbf{k}_1, k_\mu) \end{Bmatrix} \tilde{v}_\Delta(\mathbf{k}_1) \\ & + \int \frac{d\mathbf{k}_1}{(2\pi)^3} \int \frac{d\mathbf{k}_2}{(2\pi)^3} e^{i(\mathbf{k}_1+\mathbf{k}_2)\cdot\mathbf{r}} \\ & \times \begin{Bmatrix} \tilde{J}_2(\mathbf{k}_1, \mathbf{k}_2, k_\mu) \\ \tilde{K}_2(\mathbf{k}_1, \mathbf{k}_2, k_\mu) \end{Bmatrix} \tilde{v}_\Delta(\mathbf{k}_1)\tilde{v}_\Delta(\mathbf{k}_2) \\ & + \ldots . \end{aligned} \tag{7}$$

where we have introduced the reciprocal-space response functions $\tilde{J}_1(\mathbf{k}_1, k_\mu)$, $\tilde{K}_1(\mathbf{k}_1, k_\mu)$, $\tilde{J}_2(\mathbf{k}_1, \mathbf{k}_2, k_\mu)$, and $\tilde{K}_2(\mathbf{k}_1, \mathbf{k}_2, k_\mu)$, but omit their detailed formulas which appear in Sec. IV of Part I. In Eq. (7), $\tilde{v}_\Delta(\mathbf{k})$ is the Fourier transform of $v_\Delta(\mathbf{r})$ based on the convention

$$\tilde{f}(\mathbf{k}) = \int d\mathbf{r} e^{-i\mathbf{k}\cdot\mathbf{r}} f(\mathbf{r}). \tag{8}$$

The response functions in Eq. (7) are nonzero only for $\mu > v_0$. Those for the electron density have long been known in explicit form—$\tilde{J}_1(\mathbf{k}_1, k_\mu)$ was first obtained by Lindhard [18] and $\tilde{J}_2(\mathbf{k}_1, \mathbf{k}_2, k_\mu)$ was obtained by Lloyd and Sholl [37] followed by others [38–41]—and in Sec. IV of Part I we provide explicit forms for $\tilde{K}_1(\mathbf{k}_1, k_\mu)$ and $\tilde{K}_2(\mathbf{k}_1, \mathbf{k}_2, k_\mu)$. We also discuss a real-space formulation [12,42] of the response functional series in Sec. II of Part I, but, as will become clear, the conversion procedure is most natural in the reciprocal-space formulation.

III. DENSITY FUNCTIONALS AND ASSOCIATED RESPONSE FUNCTIONS

In this section, we derive the electron-density-based response functionals for the KED and the Pauli KED by applying a conversion procedure pioneered by Stoddart and March [12], to the potential functionals mentioned previously (and derived in Part I).

A. Converting potential functionals to density functionals

The conversion strategy [12] begins with consideration of the Fourier transform of the perturbed electron density from Eq. (7):

$$\begin{aligned}\tilde{n}_\Delta(\mathbf{k}) = {} & \tilde{J}_1(\mathbf{k}, k_\mu)\tilde{v}_\Delta(\mathbf{k}) \\ & + \int \frac{d\mathbf{k}_1}{(2\pi)^3} \int \frac{d\mathbf{k}_2}{(2\pi)^3} (2\pi)^3 \delta(\mathbf{k} - \mathbf{k}_1 - \mathbf{k}_2) \\ & \times \tilde{J}_2(\mathbf{k}_1, \mathbf{k}_2, k_\mu)\tilde{v}_\Delta(\mathbf{k}_1)\tilde{v}_\Delta(\mathbf{k}_2) \\ & + \sum_{m=3}^{\infty} \tilde{n}_m(\mathbf{k}),\end{aligned} \tag{9}$$

where the dependence on $\tilde{v}_\Delta(\mathbf{k})$ is left implicit in the third- and higher-order terms. Next, one rearranges this series to isolate the first appearance of $\tilde{v}_\Delta(\mathbf{k})$, yielding

$$\begin{aligned}\tilde{v}_\Delta(\mathbf{k}) = {} & \frac{\tilde{n}_\Delta(\mathbf{k})}{\tilde{J}_1(\mathbf{k}, k_\mu)} \\ & - \int \frac{d\mathbf{k}_1}{(2\pi)^3} \int \frac{d\mathbf{k}_2}{(2\pi)^3} (2\pi)^3 \delta(\mathbf{k} - \mathbf{k}_1 - \mathbf{k}_2) \\ & \times \frac{\tilde{J}_2(\mathbf{k}_1, \mathbf{k}_2, k_\mu)}{\tilde{J}_1(\mathbf{k}, k_\mu)} \tilde{v}_\Delta(\mathbf{k}_1)\tilde{v}_\Delta(\mathbf{k}_2) \\ & - \sum_{m=3}^{\infty} \frac{\tilde{n}_m(\mathbf{k})}{\tilde{J}_1(\mathbf{k}, k_\mu)}.\end{aligned} \tag{10}$$

Finally, by repeatedly inserting the left-hand side of Eq. (10) into its right-hand side, we may obtain $\tilde{v}_\Delta(\mathbf{k})$ as a functional of $\tilde{n}_\Delta(\mathbf{k})$ to arbitrary order. While the explicit expressions become unwieldy rather quickly, we may nevertheless write the result in the truncated form,

$$\begin{aligned}\tilde{v}_\Delta(\mathbf{k}) = {} & \frac{\tilde{n}_\Delta(\mathbf{k})}{\tilde{J}_1(\mathbf{k}, k_\mu)} \\ & - \int \frac{d\mathbf{k}_1}{(2\pi)^3} \int \frac{d\mathbf{k}_2}{(2\pi)^3} (2\pi)^3 \delta(\mathbf{k} - \mathbf{k}_1 - \mathbf{k}_2) \\ & \times \frac{\tilde{J}_2(\mathbf{k}_1, \mathbf{k}_2, k_\mu)}{\tilde{J}_1(\mathbf{k}, k_\mu)} \frac{\tilde{n}_\Delta(\mathbf{k}_1)}{\tilde{J}_1(\mathbf{k}_1, k_\mu)} \frac{\tilde{n}_\Delta(\mathbf{k}_2)}{\tilde{J}_1(\mathbf{k}_2, k_\mu)} \\ & + O(\tilde{n}_\Delta^3).\end{aligned} \tag{11}$$

We may now use Eq. (11) to convert the KED potential functionals in Eq. (7) into KED density functionals.

B. Kinetic energy density as a density functional

We make two notation-related comments before proceeding. In Part I, we used the symbol $t_1(\mathbf{r})$ to represent the first-order potential functional for the KED; here, as above, we use a bracket notation—$t_1[n](\mathbf{r}, k_\mu)$—to represent the analogous density functional, where it is understood that k_μ is also determined from the electron density in some fashion (see below for two possibilities), and we follow this convention wherever necessary to remove ambiguity. Second, for compactness in some expressions that follow, we use a hat syntax to refer to dimensionless response functions; for example, we define

$$\widehat{\tilde{K}_1(\mathbf{k}_1, k_\mu)} = \frac{\tilde{K}_1(\mathbf{k}_1, k_\mu)}{\tilde{K}_1(0, k_\mu)}. \tag{12}$$

1. First-order term

The first-order density functional for the KED is

$$t_1[n](\mathbf{r}, k_\mu) = \int \frac{d\mathbf{k}_1}{(2\pi)^3} e^{i\mathbf{k}_1\cdot\mathbf{r}} \tilde{Q}_1(\mathbf{k}_1, k_\mu)\tilde{n}_\Delta(\mathbf{k}_1), \tag{13}$$

where

$$\tilde{Q}_1(0, k_\mu) = \frac{k_\mu^2}{2} \tag{14}$$

and

$$\frac{\tilde{Q}_1(\mathbf{k}_1, k_\mu)}{\tilde{Q}_1(0, k_\mu)} = \frac{\widehat{\tilde{K}_1(\mathbf{k}_1, k_\mu)}}{\widehat{\tilde{J}_1(\mathbf{k}_1, k_\mu)}} = \frac{1}{2} - \frac{3\eta_1^2}{2} + [2\widehat{\tilde{J}_1(\mathbf{k}_1, k_\mu)}]^{-1}. \tag{15}$$

This functional emerges after the conversion strategy outlined above is applied to the potential functionals for the KED—see Eqs. (80) and (83) in Part I for definitions of the potential-functional components. We have not found the response function of Eqs. (14) and (15) in the literature; however, partly by coincidence, Eq. (15) happens to be very similar to (differing only by a constant shift) dimensionless integral kernels from a number of functionals that target the integrated kinetic energy or the kinetic potential—see, for example, Eq. (49) in Ref. [43], Eq. (12c) in Ref. [21], Eq. (13) in Ref. [44], and Eq. (8) in Ref. [24]—all of which originate from the second-order constraint summarized by Eq. (3) and therefore differ subtly, but essentially, from Eq. (15) in form and in meaning. We provide a plot of Eq. (15) in Fig. 1. As expected, the $\mathbf{k}_1 \to 0$ limit of the full response function,

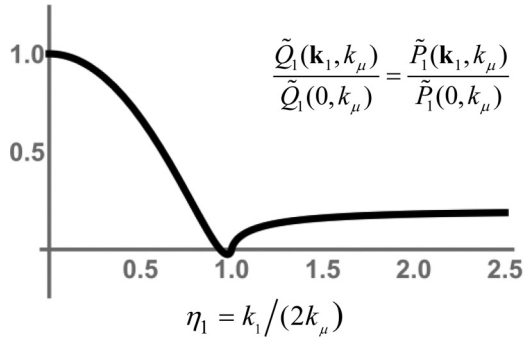

FIG. 1. Dimensionless response function governing the first-order change in the kinetic energy density (and Pauli kinetic energy density) when expressed as a density functional. The horizontal axis is normalized by a factor of k_μ, which is the Fermi wave vector associated with the reference electron density n_0. In the limit of a slowly varying perturbation ($\eta_1 \to 0$), the first-order correction to the Thomas-Fermi density functional [see Eq. (6)] is recovered. The response function has a nonanalytic feature (at $\eta_1 = 1$) and approaches 1/5 for the case of a rapidly varying perturbation ($\eta_1 \to \infty$).

Eq. (14), agrees with the first-order coefficient in Eq. (6). Finally, integrating Eq. (13) over all space yields the expected result for the first-order kinetic energy,

$$T_1[n] = \tilde{Q}_1(0, k_\mu)\tilde{n}_\Delta(0), \tag{16}$$

which vanishes if $n_\Delta(\mathbf{r})$ integrates to zero.

2. Second-order term

The second-order density functional for the KED is

$$t_2[n](\mathbf{r}, k_\mu) = \int \frac{d\mathbf{k}_1}{(2\pi)^3} \int \frac{d\mathbf{k}_2}{(2\pi)^3} \times e^{i(\mathbf{k}_1+\mathbf{k}_2)\cdot\mathbf{r}} \tilde{Q}_2(\mathbf{k}_1, \mathbf{k}_2, k_\mu)\tilde{n}_\Delta(\mathbf{k}_1)\tilde{n}_\Delta(\mathbf{k}_2), \tag{17}$$

with

$$\tilde{Q}_2(0, 0, k_\mu) = \frac{\pi^2}{2k_\mu} \tag{18}$$

and

$$\frac{\tilde{Q}_2(\mathbf{k}_1, \mathbf{k}_2, k_\mu)}{\tilde{Q}_2(0, 0, k_\mu)} = \frac{3}{2}\frac{\widehat{\tilde{K}_2(\mathbf{k}_1, \mathbf{k}_2, k_\mu)}}{\widehat{\tilde{J}_1(\mathbf{k}_1, k_\mu)}\widehat{\tilde{J}_1(\mathbf{k}_2, k_\mu)}} - \frac{1}{2}\frac{\widehat{\tilde{K}_1(\mathbf{k}_1 + \mathbf{k}_2, k_\mu)}}{\widehat{\tilde{J}_1(\mathbf{k}_1 + \mathbf{k}_2, k_\mu)}} \frac{\widehat{\tilde{J}_2(\mathbf{k}_1, \mathbf{k}_2, k_\mu)}}{\widehat{\tilde{J}_1(\mathbf{k}_1, k_\mu)}\widehat{\tilde{J}_1(\mathbf{k}_2, k_\mu)}}. \tag{19}$$

This response function, where the explicit forms of the individual components are defined in Eqs. (80), (83), (91–93), and (96–99) of Part I, is the second-order term that emerges when the conversion strategy is applied to the KED series in Eq. (7). Plots of Eq. (19) are given in Fig. 2. This function has not been reported before and is one of the primary contributions of this work. Again, the low-wave-vector limit, Eq. (18), agrees with the relevant coefficient in Eq. (6). Integration of Eq. (17)

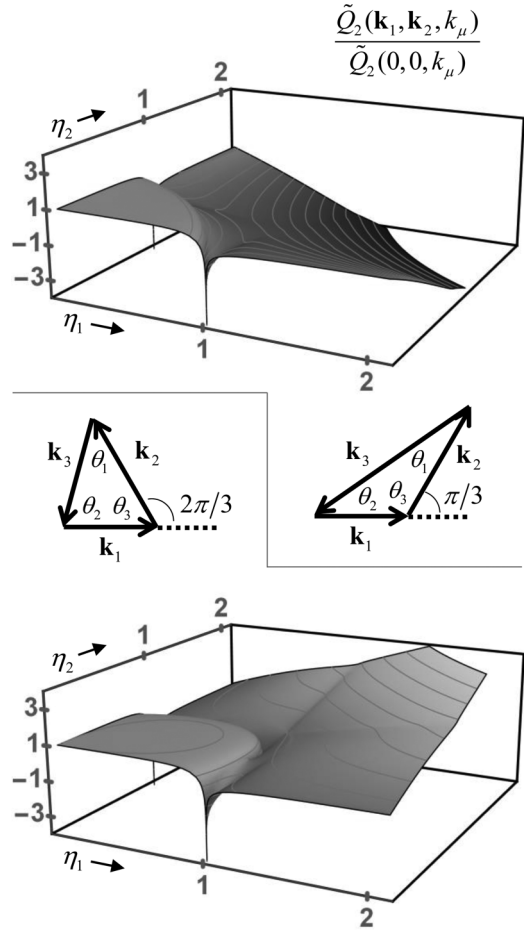

FIG. 2. Plots of the dimensionless response function [Eq. (19)] governing the second-order change in the kinetic energy density when expressed as a functional of the electron density. η_1 represents $k_1/(2k_\mu)$, and likewise for η_2. Plotted for the cases when the angle between $\mathbf{k}_1$ and $\mathbf{k}_2$ is $\pi/3$ (top) and when this angle is $2\pi/3$ (bottom). The second-order correction to the Thomas-Fermi functional [see Eq. (6)] is recovered in the $\eta_1, \eta_2 \to 0$ limit and the response function tends to diverge as $-3\boldsymbol{\eta}_1 \cdot \boldsymbol{\eta}_2$ in the $\eta_1, \eta_2 \to \infty$ limit.

over all space produces a delta function that annihilates one of the wave-vector integrals, ultimately yielding the following second-order correction to the integrated kinetic energy,

$$T_2[n] = \frac{1}{2}\int \frac{d\mathbf{k}_1}{(2\pi)^3} \frac{-1}{\tilde{J}_1(\mathbf{k}_1, k_\mu)} \tilde{n}_\Delta(\mathbf{k}_1)\tilde{n}_\Delta(-\mathbf{k}_1), \tag{20}$$

which is in accord with Eq. (3). Finally, close inspection of Eq. (19)—not given here in detail, but see Fig. 2—reveals that $\tilde{Q}_2(\mathbf{k}_1, \mathbf{k}_2, k_\mu)$ behaves asymptotically as $-\mathbf{k}_1 \cdot \mathbf{k}_2/(8n_0)$ when $\mathbf{k}_1$ and $\mathbf{k}_2$ are large, a point to which we return shortly.

C. Pauli kinetic energy density as a density functional

As noted above, the von Weizsäcker KED is known explicitly as a density functional, and so one may choose to develop approximations for the Pauli KED rather than the full KED. Here, we adapt functionals given previously into approximations for the Pauli KED [$t_0^P[n_0]$, $t_1^P[n](\mathbf{r}, k_\mu)$, and

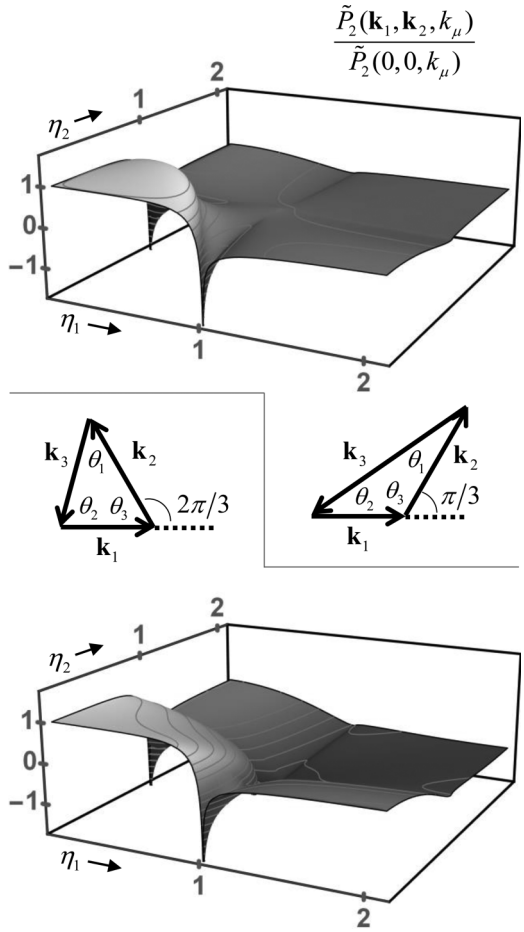

FIG. 3. Plots of the dimensionless response function [Eq. (24)] governing the second-order change in the Pauli kinetic energy density when expressed as a functional of the electron density. η_1 represents $k_1/(2k_\mu)$, and likewise for η_2. Plotted for the cases when the angle between $\mathbf{k}_1$ and $\mathbf{k}_2$ is $\pi/3$ (top) and when this angle is $2\pi/3$ (bottom). The second-order correction to the Thomas-Fermi functional [see Eq. (6)] is recovered in the $\eta_1, \eta_2 \to 0$ limit and the response function remains finite in the $\eta_1, \eta_2 \to \infty$ limit.

$t_2^P[n](\mathbf{r}, k_\mu)$]. If, beginning with $t_{vW}[n](\mathbf{r})$ as given by Eq. (2), one conducts a functional Taylor expansion (see the appendices in Ref. [45] or Ref. [46]) about a uniform reference density through second order, then the zeroth- and first-order terms vanish and the result is

$$t_{vW}[n](\mathbf{r}) \approx \frac{|\nabla n_\Delta(\mathbf{r})|^2}{8n_0} + O\left(n_\Delta^3\right). \tag{21}$$

For this reason, free-electron-based response functionals for the Pauli KED only begin to differ from those for the full KED at second order—for example, $t_0^P[n_0] = t_0[n_0]$. Furthermore, the second-order term shown in Eq. (21), when converted to Fourier space, is precisely the divergent $-\mathbf{k}_1 \cdot \mathbf{k}_2/(8n_0)$ term that we highlighted in the sentence following Eq. (19). When this term is subtracted from Eq. (19) to yield the second-order correction in the Pauli KED, the resulting function remains finite when $\mathbf{k}_1$ and $\mathbf{k}_2$ are large (see Fig. 3).

1. First-order term

The first-order density functional for the Pauli KED is

$$t_1^P[n](\mathbf{r}, k_\mu) = \int \frac{d\mathbf{k}_1}{(2\pi)^3} e^{i\mathbf{k}_1\cdot\mathbf{r}} \tilde{P}_1(\mathbf{k}_1, k_\mu)\tilde{n}_\Delta(\mathbf{k}_1), \tag{22}$$

where $\tilde{P}_1(\mathbf{k}_1, k_\mu) = \tilde{Q}_1(\mathbf{k}_1, k_\mu)$ and $\tilde{Q}_1(\mathbf{k}_1, k_\mu)$ is the first-order correction to the full KED given in Eq. (15).

2. Second-order term

The second-order density functional for the Pauli KED is

$$t_2^P[n](\mathbf{r}, k_\mu) = \int \frac{d\mathbf{k}_1}{(2\pi)^3} \int \frac{d\mathbf{k}_2}{(2\pi)^3} \times e^{i(\mathbf{k}_1+\mathbf{k}_2)\cdot\mathbf{r}} \tilde{P}_2(\mathbf{k}_1, \mathbf{k}_2, k_\mu)\tilde{n}_\Delta(\mathbf{k}_1)\tilde{n}_\Delta(\mathbf{k}_2) \tag{23}$$

with $\tilde{P}_2(0, 0, k_\mu) = \tilde{Q}_2(0, 0, k_\mu)$ and

$$\frac{\tilde{P}_2(\mathbf{k}_1, \mathbf{k}_2, k_\mu)}{\tilde{P}_2(0, 0, k_\mu)} = \frac{\tilde{Q}_2(\mathbf{k}_1, \mathbf{k}_2, k_\mu)}{\tilde{Q}_2(0, 0, k_\mu)} + 3\eta_1 \cdot \eta_2. \tag{24}$$

As noted above, Eq. (24) remains finite as $\mathbf{k}_1$ and $\mathbf{k}_2$ become large. Equation (24) is plotted in Fig. 3.

IV. TESTING THE ELECTRON-DENSITY-BASED RESPONSE FUNCTIONALS FOR THE KINETIC ENERGY DENSITY

In this section, we apply the electron-density-based response functionals for the KED and Pauli KED to electron densities associated with a few crystalline solids. The test systems are local electron-ion pseudopotential models of body-centered cubic Li, face-centered cubic Al, and cubic diamond Si. We obtained the test system benchmark data from KSDFT calculations conducted with the ABINIT code [47] using a generalized gradient approximation (GGA) [48] for the XC functional. To ensure high resolution in the local properties, we used very high computational settings [3200 eV for the plane-wave kinetic energy cutoff, $32 \times 32 \times 32$ k-point meshes for unit cells of two (Li), four (Al), and two (Si) atoms, and Fermi-Dirac smearing of 0.01 eV]. The local pseudopotentials for Li and Si were the same as those used in Ref. [49] and the local pseudopotential for Al was the same as that used in Ref. [50]—see Ref. [51].

We summarize the test system data in Figs. 4–6, giving the converged KS effective potential, KS electron density, and KS KED, all along the [111] direction of the cubic unit cell. We keep these properties fixed for the remainder of the analysis (without adjusting them self-consistently), and so the KS effective potential may be viewed simply as an applied external potential. (After accounting for ion-ion interactions, the crystals are charge-neutral; therefore, the spatial average of these potentials has no Coulombic contribution and derives entirely from non-Coulombic parts of the respective local pseudopotentials as well as XC effects.) In Figs. 4–6, we also show the Fermi energy of the highest occupied orbital, the free-electron KED obtained by inserting the average electron density for the respective system into the Thomas-Fermi functional given by Eq. (5), and the von Weizsäcker KED given by Eq. (2).

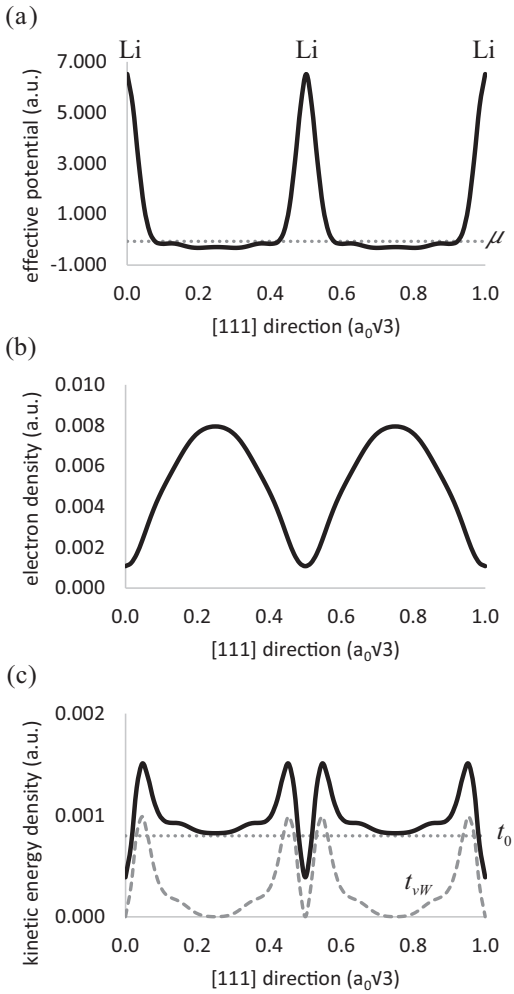

FIG. 4. For body-centered cubic Li modeled with a local pseudopotential and GGA XC, plots of (a) the effective external potential $v(\mathbf{r})$, (b) the electron density $n(\mathbf{r})$, and (c) the KED $t(\mathbf{r})$ along the [111] diagonal of the cubic unit cell, derived from KSDFT calculations. In each plot, the horizontal axis is scaled by a factor of the lattice constant a_0 and the vertical axis is expressed in Hartree atomic units. In (a), Li atom locations are marked with "Li" and the Fermi energy μ is shown as a dotted line. Electrons must tunnel to traverse the classically forbidden regions where $v(\mathbf{r}) > \mu$. In (c), the free-electron KED $t_0[n_0]$, obtained by inserting the average electron density into the Thomas-Fermi functional, is shown as a dotted line, and the von Weizsäcker KED $t_{vW}[n](\mathbf{r})$ is shown as a dashed curve.

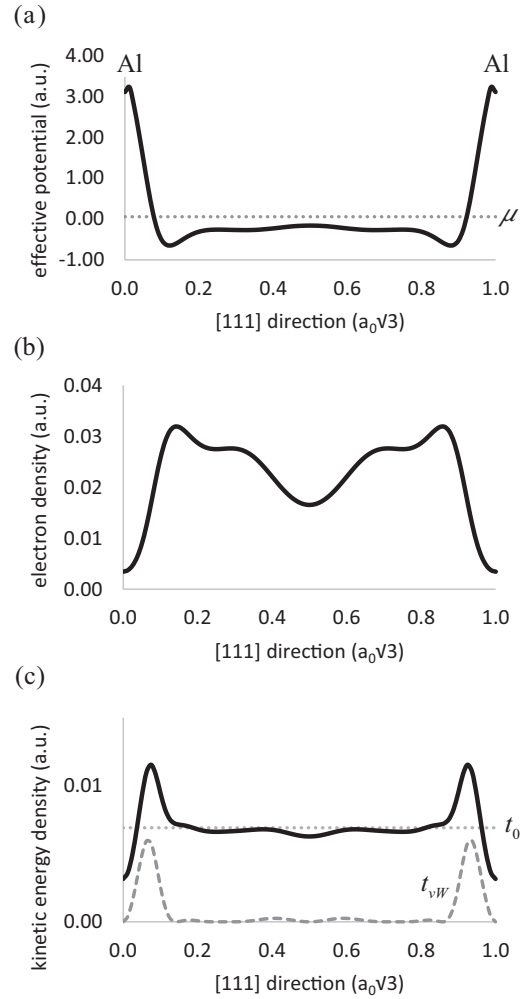

FIG. 5. For face-centered cubic Al modeled with a local pseudopotential and GGA XC, plots of (a) the effective external potential $v(\mathbf{r})$, (b) the electron density $n(\mathbf{r})$, and (c) the KED $t(\mathbf{r})$ along the [111] diagonal of the cubic unit cell, derived from KSDFT calculations. In each plot, the horizontal axis is scaled by a factor of the lattice constant a_0 and the vertical axis is expressed in Hartree atomic units. In (a), Al atom locations are marked with "Al" and the Fermi energy μ is shown as a dotted line. Electrons must tunnel to traverse the classically forbidden regions where $v(\mathbf{r}) > \mu$. In (c), the free-electron KED $t_0[n_0]$, obtained by inserting the average electron density into the Thomas-Fermi functional, is shown as a dotted line, and the von Weizsäcker KED $t_{vW}[n](\mathbf{r})$ is shown as a dashed curve.

In Figs. 7–9, we summarize the response functional estimates to the KED and Pauli KED for the three test systems based on the KS electron densities shown in Figs. 4–6, which are held fixed. For comparison, the exact KEDs from Figs. 4–6 are reproduced in Figs. 7–9, with the latter plots just showing more detail over a smaller region. Figure 7(a), Fig. 8(a), and Fig. 9(a) are based on the following approximation to $t(\mathbf{r})$ involving the response functionals for the full KED:

$$t(\mathbf{r}) \approx t_0[n_0] + t_1[n](\mathbf{r}, k_\mu[n_0]) + t_2[n](\mathbf{r}, k_\mu[n_0]), \quad (25)$$

where n_0 refers to the average electron density for the respective system, and $t_1[n](\mathbf{r}, k_\mu[n_0])$ and $t_2[n](\mathbf{r}, k_\mu[n_0])$ are computed from Eqs. (13)–(15) and Eqs. (17)–(19), respectively. Figure 7(b), Fig. 8(b), and Fig. 9(b) are based on a different approximation for $t(\mathbf{r})$ involving the von Weizsäcker KED and response functionals for the Pauli KED:

$$t(\mathbf{r}) \approx t_{vW}[n](\mathbf{r}) + t_0^P[n_0] + t_1^P[n](\mathbf{r}, k_\mu[n_0]) + t_2^P[n](\mathbf{r}, k_\mu[n_0]), \quad (26)$$

where $t_{vW}[n](\mathbf{r})$ is computed from Eq. (2), n_0 is again the average electron density, and $t_1^P[n](\mathbf{r}, k_\mu[n_0])$ and $t_2^P[n](\mathbf{r}, k_\mu[n_0])$ are determined from Eq. (22) and Eqs. (23)–(24), respectively. In essentially every case, the approximation of Eq. (26) is markedly better than the approximation of Eq. (25), seemingly because Eq. (26) includes the full von Weizsäcker

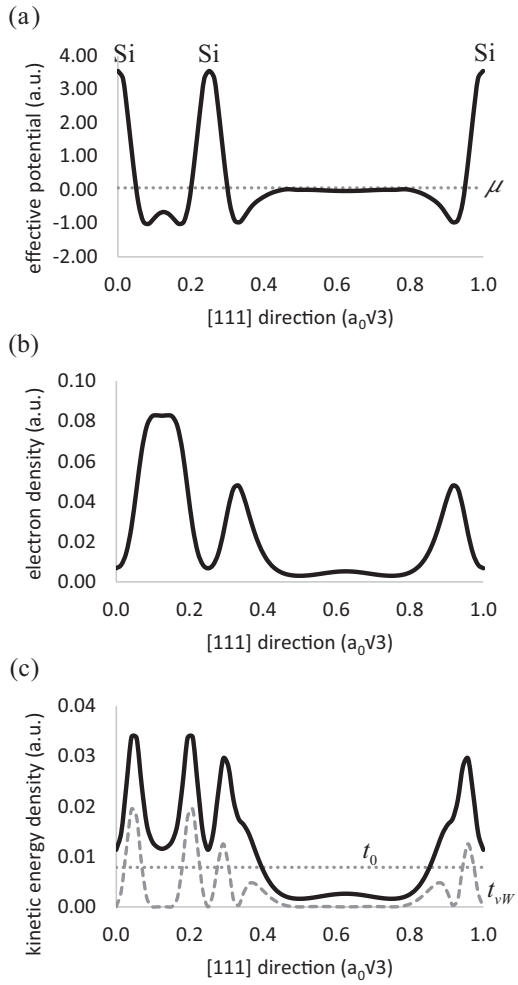

FIG. 6. For cubic diamond Si modeled with a local pseudopotential and GGA XC, plots of (a) the effective external potential $v(\mathbf{r})$, (b) the electron density $n(\mathbf{r})$, and (c) the KED $t(\mathbf{r})$ along the [111] diagonal of the cubic unit cell, derived from KSDFT calculations. In each plot, the horizontal axis is scaled by a factor of the lattice constant a_0 and the vertical axis is expressed in Hartree atomic units. In (a), Si atom locations are marked with "Si" and the Fermi energy μ is shown as a dotted line. Electrons must tunnel to traverse the classically forbidden regions where $v(\mathbf{r}) > \mu$. In (c), the free-electron KED $t_0[n_0]$, obtained by inserting the average electron density into the Thomas-Fermi functional, is shown as a dotted line, and the von Weizsäcker KED $t_{vW}[n](\mathbf{r})$ is shown as a dashed curve.

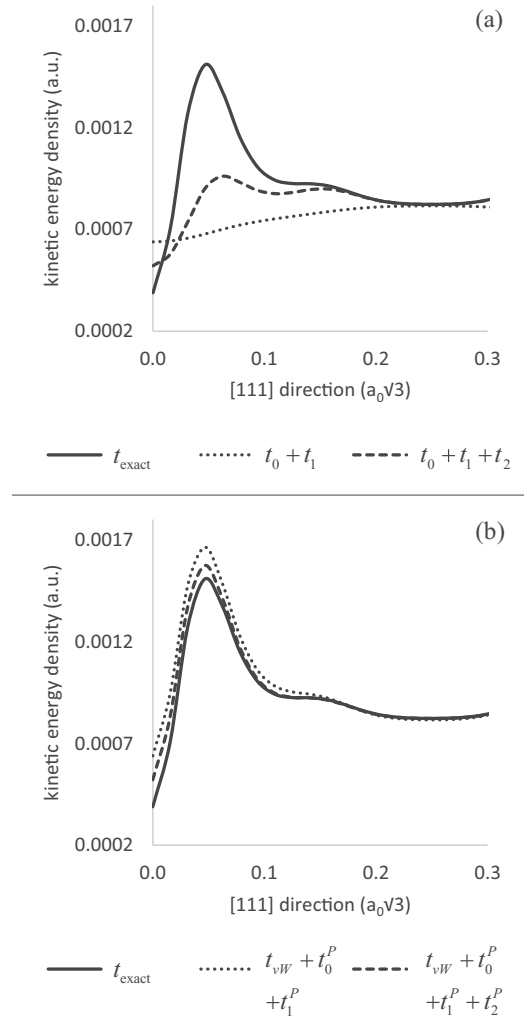

FIG. 7. Response functional approximations for the KED of the body-centered cubic Li test system (Fig. 4). In (a), the exact KED (solid curve, reproduced from Fig. 4) is compared with the first- and second-order density functional estimates for the full KED (dotted and dashed curves, respectively)—see Eq. (25). In (b), the exact KED (solid curve) is compared with the sum of the von Weizsäcker KED and the first- and second-order density functional estimates for the remaining Pauli KED (dotted and dashed curves, respectively)—see Eq. (26). In both (a) and (b), the approximations are accurate in the free-electron-like region; however, only in (b) are the approximations also reasonably accurate in the classically forbidden region.

term while Eq. (25) only includes a second-order approximation to the von Weizsäcker term. Put differently, Eq. (26) constitutes a partial resummation of the perturbation series in which the portion of the series leading to the von Weizsäcker term is summed to infinite order and the remaining part (the Pauli KED) is approximated through second order. Moreover, in all cases, inclusion of the second-order term yields demonstrable improvement over the first-order-accurate approximations. In particular, both first-order approximations generate a negative KED in the low-density regions of the Si test system (Fig. 9), in clear violation of the local $t(\mathbf{r}) \geqslant t_{vW}[n](\mathbf{r})$ constraint, and that this defect is remedied by inclusion of the second-order terms.

Thus far, all approximations have relied on a fixed n_0 for determining first- and second-order corrections, where n_0 has been set as the average electron density of the system under consideration. A natural alternative is to use the local $n(\mathbf{r})$ as the reference density for the location $\mathbf{r}$. The zeroth-order Pauli KED, for example, is the local Thomas-Fermi KED in this case instead of the constant $t_0^P[n_0]$, and the full second-order-accurate approximation originally given by Eq. (26) becomes

$$t(\mathbf{r}) \approx t_{vW}[n](\mathbf{r}) + t_{TF}[n](\mathbf{r}) + t_1^P[n](\mathbf{r}, k_\mu[n](\mathbf{r})) + t_2^P[n](\mathbf{r}, k_\mu[n](\mathbf{r})). \quad (27)$$

This revised approximation, because of the additional density dependence in the response functions, is more challenging to

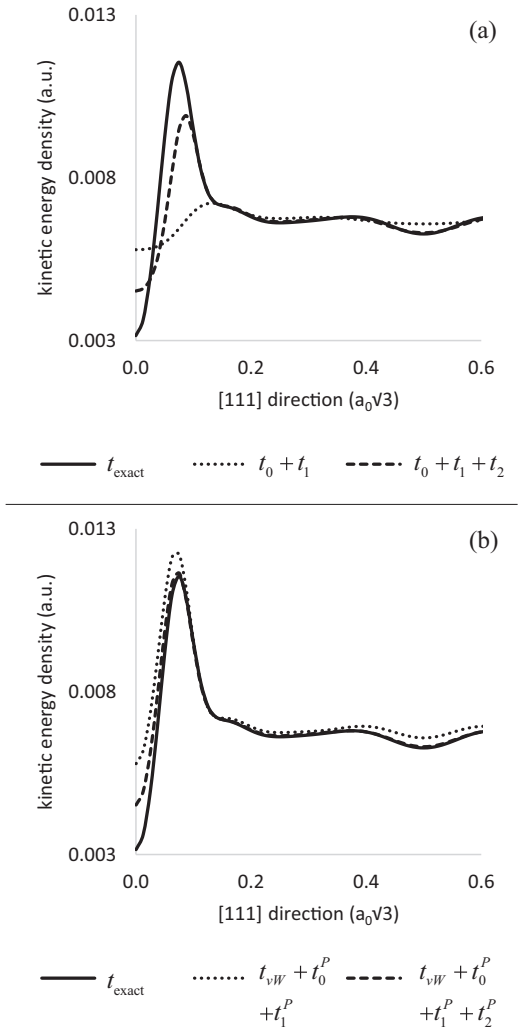

FIG. 8. Response functional approximations for the KED of the face-centered cubic Al test system (Fig. 5). In (a), the exact KED (solid curve, reproduced from Fig. 5) is compared with the first- and second-order density functional estimates for the full KED (dotted and dashed curves, respectively)—see Eq. (25). In (b), the exact KED (solid curve) is compared with the sum of the von Weizsäcker KED and the first- and second-order density functional estimates for the remaining Pauli KED (dotted and dashed curves, respectively)—see Eq. (26). In both (a) and (b), the approximations are accurate in the free-electron-like region; however, only in (b) are the approximations also reasonably accurate in the classically forbidden region.

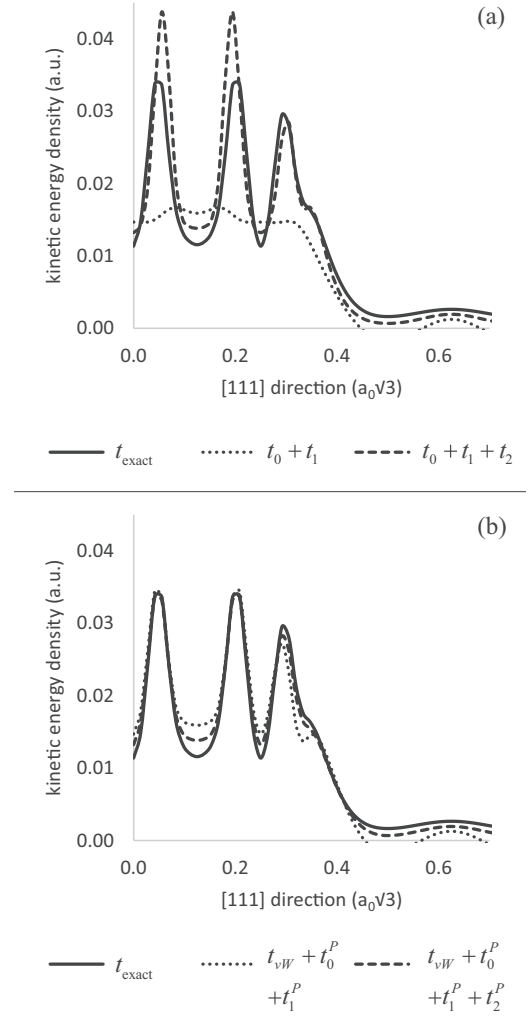

FIG. 9. Response functional approximations for the KED of the cubic diamond Si test system (Fig. 6). In (a), the exact KED (solid curve, reproduced from Fig. 6) is compared with the first- and second-order density functional estimates for the full KED (dotted and dashed curves, respectively)—see Eq. (25). In (b), the exact KED (solid curve) is compared with the sum of the von Weizsäcker KED and the first- and second-order density functional estimates for the remaining Pauli KED (dotted and dashed curves, respectively)—see Eq. (26). In both (a) and (b), the second-order approximations are relatively accurate in the free-electron-like regions, but the first-order approximations are insufficient, as judged by unphysically negative estimates for the KED at some locations. Only in (b) are the approximations reasonably accurate in the classically forbidden regions.

evaluate than the original. The usual approach [26,52,53] for keeping the computational expense manageable for such functionals (having single-density-dependent kernels) involves computing $t_1^P[n](\mathbf{r}, k_\mu[n_j])$ for a discrete set of n_j values and then extending these results to arbitrary values of $n(\mathbf{r})$ with interpolating splines. In Fig. 10, the results of applying of Eq. (27) to the three test systems are reported, based on uniform spacing of 0.0025 a.u. between successive n_j values and linear splines.

With this approximation, the results for the Li test system [Fig. 10(a)] are excellent for both the first- and second-order accurate versions. For the Al test system [Fig. 10(b)], the first-order-accurate result improves on the previous first-order (fixed-reference-density) approximation [Fig. 8(b)]; however, the second-order result in Fig. 10(b) displays some irregularities. This problem becomes more severe for the Si test system [Fig. 10(c)], for which the second-order-accurate approximation becomes significantly worse than the first-order approximation in some regions. Referring to Fig. 6, one sees that the unphysical behavior occurs where the local electron density is very low, suggesting an explanation: If the free-electron reference density is very small compared with the fluctuations in the electron density, the convergence of the perturbation series is imperiled.

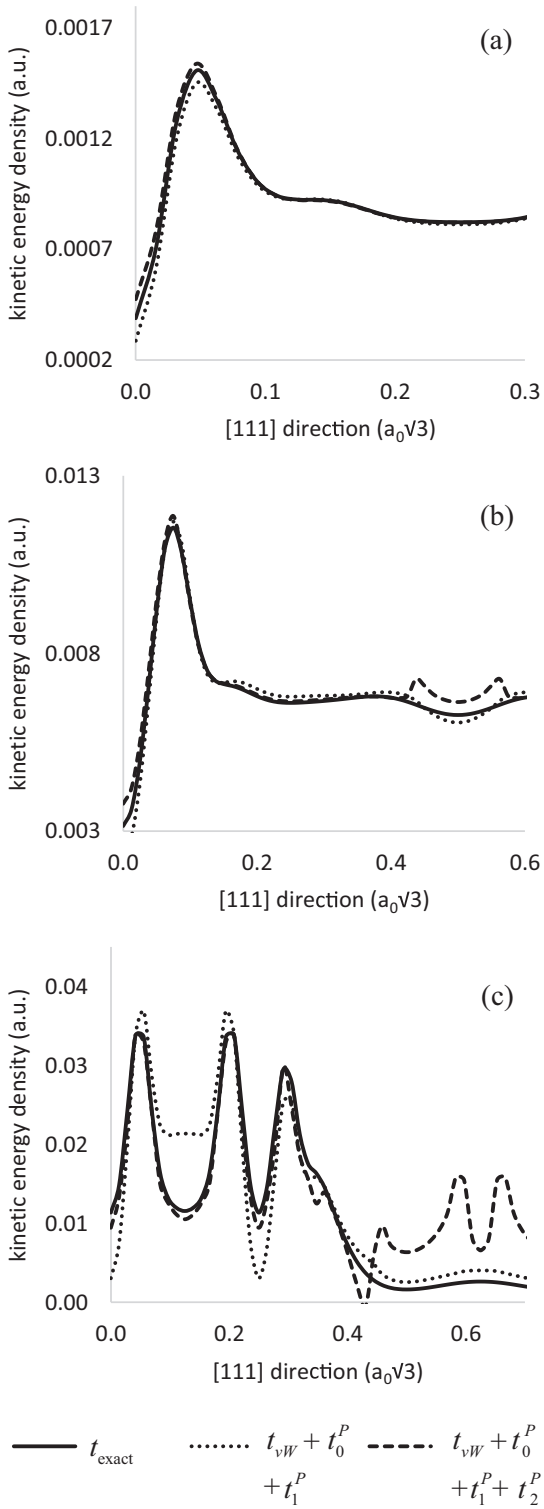

FIG. 10. Response functional approximations for the KED utilizing a locally adjusted free-electron reference density. In (a), (b), and (c), respectively, the exact KEDs for the Li, Al, and Si systems (solid curves, reproduced from Figs. 4, 5, and 6) are compared with the sum of the von Weizsäcker KED and the first- and second-order-accurate density functional estimates for the Pauli KED (dotted and dashed curves, respectively). In contrast with the fixed-reference-density approximations appearing in Figs. 7(b), 8(b), and 9(b), the latter functionals are evaluated using a locally adjusted reference density—see Eq. (27).

V. CONCLUDING REMARKS

In this second paper of the two-part series, we considered electron-density-based response functionals for the nonnegative KED of nearly free electrons. Using the potential functionals developed in Part I, we derived the first- and second-order corrections to the free-electron KED as functionals of the electron density. The reciprocal-space integral kernels we provided supply physical insight and are of practical value because they enable more efficient evaluation of the functionals via fast Fourier transform (FFT) techniques. The first-order response function for the full KED, Eq. (15), is fairly simple, but the second-order function, Eqs. (18) and (19), is considerably more difficult to obtain, requiring the function $\tilde{K}_2(\mathbf{k}_1, \mathbf{k}_2, k_\mu)$ derived at length in Part I. Finally, we also provided density functionals for the first- and second-order response in the Pauli KED—Eq. (22) and Eqs. (23)–(24), respectively—which is the non-negative amount in excess of the von Weizsäcker KED. The first-order functional for the Pauli KED is identical to that of the full KED, whereas the second-order functionals differ by a simple term.

In Sec. IV, we examined approximate KEDs generated by electron-density-based response functionals when applied to KS electron densities derived from local pseudopotential models of body-centered cubic Li, face-centered cubic Al, and cubic diamond Si. In general, particularly when the second-order term is included, they provide reasonable approximations to the exact $t(\mathbf{r})$ in free-electron-like regions where the electron density deviates only modestly from uniformity. However, the combination of the von Weizsäcker KED with response functional approximations for the remaining Pauli KED yields a marked improvement in regions where the electron density varies more rapidly. This observation regarding the local KED helps explain the success of approximations for the integrated kinetic energy that involve the full von Weizsäcker energy and obey the constraint specified by Eq. (3). We also investigated adjusting the free-electron reference density locally and observed apparent nonconvergence of the perturbation series in regions where the local density is much smaller than the overall magnitude of density fluctuations.

We anticipate that knowledge of the structure of the KED response functionals will help guide the design of more sophisticated kinetic energy density functionals that enable more accurate OFDFT simulations of materials. For example, Eqs. (17)–(19) imply a constraint on density functional estimates for $t(\mathbf{r})$ that represents a local generalization of Eq. (3). One immediate possibility for follow-up involves finding techniques for evaluating Eq. (17) and/or Eq. (23) with a computational effort that scales linearly with system size because direct evaluation of these expressions incurs no better than quadratic scaling, even with assistance from FFT techniques. This problem has been solved (approximately) in a slightly different context [20,23] and we are currently exploring this possibility. Another obvious avenue for follow-up involves greater consideration of location-dependent reference electron densities—for example, with the response functions for the local KED (or Pauli KED) provided in this paper, one may easily consider the generalization $n_0 \rightarrow \tilde{n}(\mathbf{r})$. We explored the simplest choice briefly in Sec. IV, which is to define $\tilde{n}(\mathbf{r}) \equiv$

$n(\mathbf{r})$ in the spirit of the Thomas-Fermi approximation such that $t_0(\mathbf{r}) \equiv t_{TF}[n](\mathbf{r})$. However, it seems likely that choosing $\tilde{n}(\mathbf{r})$ in a more sophisticated manner would yield better results. Finally, while the frozen-density calculations we presented in Sec. IV are useful for conceptual and diagnostic purposes, additional insight would follow from self-consistent OFDFT calculations during which the electron density is varied until the total system energy is minimized. These computations require kinetic potentials obtained by straightforward functional differentiation of our results. Such self-consistent calculations represent a more rigorous test for OF functionals because the approximations must work reasonably well for all trial densities; if not, the OF-derived density may differ significantly from the KS density, increasing the overall error.

Note added in proof: We thank an anonymous referee for bringing to our attention Ref. [54], which outlines an alternate method of achieving the inversion from potential functionals to density functionals.

ACKNOWLEDGMENTS

We thank N. Baughman and Dr. B. G. del Rio, Dr. X. Zhang, and Dr. K. Jiang for reviewing versions of this manuscript and acknowledge support from the Office of Naval Research (Grant No. N00014-15-1-2218).

APPENDIX

Here, we demonstrate that the conventional gradient expansion for the KED (in density-functional form) is encoded in the response functional formalism that is the subject of this work. Using the fact that

$$\frac{1}{\widetilde{J_1(\mathbf{k}_1 \to 0, k_\mu)}} \approx 1 + \frac{1}{3}\eta_1^2 + \frac{8}{45}\eta_1^4, \tag{A1}$$

together with the asymptotic forms of the potential-based response functions given in Sec. V of Part I, one can show that

$$\frac{\tilde{Q}_1(\mathbf{k}_1 \to 0, k_\mu)}{\tilde{Q}_1(0, k_\mu)} \approx 1 - \frac{4}{3}\eta_1^2 + \frac{4}{45}\eta_1^4 \tag{A2}$$

and

$$\begin{aligned}\frac{\tilde{Q}_2(\mathbf{k}_1 \to 0, \mathbf{k}_2 \to 0, k_\mu)}{\tilde{Q}_2(0, 0, k_\mu)} &\approx 1 - \frac{1}{3}\boldsymbol{\eta}_1 \cdot \boldsymbol{\eta}_2 - \frac{4}{45}\left(\eta_1^4 + \eta_2^4\right) \\ &\quad - \frac{1}{3}(\eta_1^2 + \eta_2^2)\boldsymbol{\eta}_1 \cdot \boldsymbol{\eta}_2 - \frac{14}{45}\eta_1^2\eta_2^2 - \frac{7}{45}(\boldsymbol{\eta}_1 + \boldsymbol{\eta}_2)^2\boldsymbol{\eta}_1 \cdot \boldsymbol{\eta}_2.\end{aligned} \tag{A3}$$

Using these results, together with Eqs. (5), (13), and (17), one may further show that

$$\begin{aligned}t(\mathbf{r}) \approx c_0 n^{5/3}(\mathbf{r}) + \frac{1}{6}\nabla^2 n(\mathbf{r}) + \frac{1}{72}\frac{|\nabla n(\mathbf{r})|^2}{n(\mathbf{r})} \\ + \frac{(\nabla^2)^2 n(\mathbf{r})}{1200 c_0 n^{2/3}(\mathbf{r})} - \frac{\nabla[\nabla^2 n(\mathbf{r})] \cdot \nabla n(\mathbf{r})}{480 c_0 n^{5/3}(\mathbf{r})} \\ - \frac{7[\nabla^2 n(\mathbf{r})]^2}{7200 c_0 n^{5/3}(\mathbf{r})} - \frac{7\nabla^2[|\nabla n(\mathbf{r})|^2]}{14400 c_0 n^{5/3}(\mathbf{r})}.\end{aligned} \tag{A4}$$

The terms involving two derivatives in Eq. (A4) comprise the full second-order gradient expansion (compare with Eq. 5.50 in Ref. [13]), and the terms involving four derivatives in Eq. (A4) are identical to terms appearing in the fourth-order gradient expansion (compare with Eq. 5.51 in Ref. [13]). To recover the entire fourth-order gradient expansion, one would need to carry out the response functional formalism through fourth order.

[1] W. C. Witt and E. A. Carter, Phys. Rev. B **100**, 125106 (2019).
[2] N. H. March, Phys. Lett. A **113**, 476 (1986).
[3] M. Levy and H. Ou-Yang, Phys. Rev. A **38**, 625 (1988).
[4] C. F. von Weizsäcker, Z. Phys. **96**, 431 (1935).
[5] S. Kurth, J. P. Perdew, and P. Blaha, Int. J. Quantum Chem. **75**, 889 (1999).
[6] P. Hohenberg and W. Kohn, Phys. Rev. **136**, B864 (1964).
[7] W. Kohn and L. J. Sham, Phys. Rev. **140**, A1133 (1965).
[8] Y. A. Wang and E. A. Carter, in *Theoretical Methods in Condensed Phase Chemistry* (Springer, Dordrecht, 2002), pp. 117–184.
[9] *Recent Progress in Orbital-Free Density Functional Theory*, edited by T. A. Wesolowski and Y. A. Wang (World Scientific, Singapore, 2013).
[10] V. V. Karasiev, D. Chakraborty, and S. B. Trickey, in *Many-Electron Approaches in Physics, Chemistry and Mathematics* (Springer, Cham, 2014), pp. 113–134.
[11] W. C. Witt, B. G. del Rio, J. M. Dieterich, and E. A. Carter, J. Mater. Res. **33**, 777 (2018).
[12] J. C. Stoddart and N. H. March, Proc. R. Soc. London, Ser. A **299**, 279 (1967).
[13] R. M. Dreizler and E. K. U. Gross, *Density Functional Theory: An Approach to the Quantum Many-Body Problem* (Springer Science & Business Media, Berlin, 1990).
[14] A. A. Kugler, Phys. Rev. A **41**, 3489 (1990).
[15] J. Shao, Mod. Phys. Lett. B **07**, 1193 (1993).
[16] E. V. Ludeña and V. V. Karasiev, Rev. Mod. Quantum Chem. **1**, 612 (2002).
[17] D. García-Aldea and J. E. Alvarellos, in *Theoretical and Computational Developments in Modern Density Functional Theory*, edited by A. K. Roy (Nova Science, Hauppauge, NY, 2012).
[18] J. Lindhard, K. Dan. Vidensk. Selsk., Mat.-Fys. Medd. **28**, 1 (1954).
[19] E. Chacón, J. E. Alvarellos, and P. Tarazona, Phys. Rev. B **32**, 7868 (1985).
[20] L.-W. Wang and M. P. Teter, Phys. Rev. B **45**, 13196 (1992).
[21] F. Perrot, J. Phys.: Condens. Matter **6**, 431 (1994).
[22] E. Smargiassi and P. A. Madden, Phys. Rev. B **49**, 5220 (1994).
[23] M. Foley and P. A. Madden, Phys. Rev. B **53**, 10589 (1996).

[24] J.-D. Chai, V. L. Lignères, G. Ho, E. A. Carter, and J. D. Weeks, Chem. Phys. Lett. **473**, 263 (2009).
[25] W. Mi, A. Genova, and M. Pavanello, J. Chem. Phys. **148**, 184107 (2018).
[26] C. Huang and E. A. Carter, Phys. Rev. B **81**, 045206 (2010).
[27] L. A. Constantin, E. Fabiano, and F. Della Sala, Phys. Rev. B **97**, 205137 (2018).
[28] L. A. Constantin, E. Fabiano, and F. Della Sala, J. Phys. Chem. Lett. **9**, 4385 (2018).
[29] K. Luo, V. V. Karasiev, and S. B. Trickey, Phys. Rev. B **98**, 041111(R) (2018).
[30] A. V. Bienvenu and G. Knizia, J. Chem. Theor. Comput. **14**, 1297 (2018).
[31] F. Tran, P. Kovács, L. Kalantari, G. K.H. Madsen, and P. Blaha, J. Chem. Phys. **149**, 144105 (2018).
[32] D. Mejia-Rodriguez and S. B. Trickey, Phys. Rev. B **98**, 115161 (2018).
[33] Y. Ke, F. Libisch, J. Xia, L.-W. Wang, and E. A. Carter, Phys. Rev. Lett. **111**, 066402 (2013).
[34] Y. Ke, F. Libisch, J. Xia, and E. A. Carter, Phys. Rev. B **89**, 155112 (2014).
[35] L. H. Thomas, Math. Proc. Cambridge Philos. Soc. **23**, 542 (1927).
[36] E. Fermi, Rend. Accad. Naz. Lincei **6**, 32 (1927).
[37] P. Lloyd and C. A. Sholl, J. Phys. C Solid State Phys. **1**, 1620 (1968).
[38] E. G. Brovman, Yu. Kagan, and A. Kholas, Sov. J. Exp. Theor. Phys. **34**, 394 (1972).
[39] J. Hammerberg and N. W. Ashcroft, Phys. Rev. B **9**, 409 (1974).
[40] A. Milchev and R. Pickenhain, Phys. Status Solidi B **79**, 549 (1977).
[41] S. Li and J. K. Percus, J. Math. Phys. **32**, 776 (1991).
[42] N. H. March and A. M. Murray, Proc. R. Soc. London, Ser. A **261**, 119 (1961).
[43] C. Herring, Phys. Rev. A **34**, 2614 (1986).
[44] Y. A. Wang, N. Govind, and E. A. Carter, Phys. Rev. B **60**, 16350 (1999).
[45] R. G. Parr and W. Yang, *Density-Functional Theory of Atoms and Molecules* (Oxford University Press, Oxford, 1994).
[46] E. Engel and R. M. Dreizler, *Density Functional Theory: An Advanced Course* (Springer Science & Business Media, Berlin, 2011).
[47] X. Gonze, F. Jollet, F. Abreu Araujo, D. Adams, B. Amadon, T. Applencourt, C. Audouze, J.-M. Beuken, J. Bieder, A. Bokhanchuk, E. Bousquet, F. Bruneval, D. Caliste, M. Côté, F. Dahm, F. Da Pieve, M. Delaveau, M. Di Gennaro, B. Dorado, and C. Espejo *et al.*, Comput. Phys. Commun. **205**, 106 (2016).
[48] J. P. Perdew, K. Burke, and M. Ernzerhof, Phys. Rev. Lett. **77**, 3865 (1996).
[49] J. Xia and E. A. Carter, J. Power Sources **254**, 62 (2014).
[50] J. Xia and E. A. Carter, Phys. Rev. B **91**, 045124 (2015).
[51] https://github.com/PrincetonUniversity/BLPSLibrary (2019).
[52] G. Román-Pérez and J. M. Soler, Phys. Rev. Lett. **103**, 096102 (2009).
[53] W. Mi and M. Pavanello, Phys. Rev. B **100**, 041105(R) (2019).
[54] L. Šamaj and J. K. Percus, J. Chem. Phys. **111**, 1809 (1999).